

Chapter 4

Optical properties of antiferroelectric liquid crystals

4.1 Introduction

The orientational order in the liquid crystalline phases coupled with the anisotropy of the constituent molecules gives rise to strong anisotropies in their macroscopic properties. For instance the magnetic susceptibility, refractive index and electrical conductivity are highly anisotropic in these phases. The anisotropy in the refractive index and the rich variety of structures of the liquid crystalline phases which can be easily changed by external means give rise to many interesting optical effects. On the one hand these optical properties are employed for applications in liquid crystal display (LCD) devices and on the other hand polarized light is often used as a probe to investigate the structures of these phases. Many optical measurements using a variety of powerful techniques such as polarized light microscopy, conoscopy, ellipsometry, circular dichroism, optical rotatory power measurements, Rayleigh scattering and photon correlation spectroscopy are used for this purpose.

As we have mentioned in previous chapters the compounds exhibiting the antiferroelectric SmC_A^* phase also exhibit a number of ferrielectric and other sub-phases as the temperature is varied. We have shown in chapter 2 that our discrete model can account for all these sub-phases exhibited by antiferroelectric liquid crystals. Further, in Chapter 3 we have calculated the effect of an external static electric field on the structures of these phases and it is shown that the calculated apparent tilt angle θ_{app} agrees well with the experimental variations. In this chapter we will describe calculations of conoscopic patterns, ellipsometric parameters and optical rotatory power corresponding to the different structures predicted by our model and compare the results with the experimental observations.

Conoscopic observations have been extensively used in elucidating the characteristic changes in the structures of the various phases exhibited by AFLC as a function of an in-plane static electric field (for a general introduction to conoscopy see Sec. 4.3.1). Fig. 4.1 shows the conoscopic figures obtained experimentally by Gorecka et al. [15] for homeotropically aligned AFLC sample (MHPOBC) in various phases. The thickness of the cell used

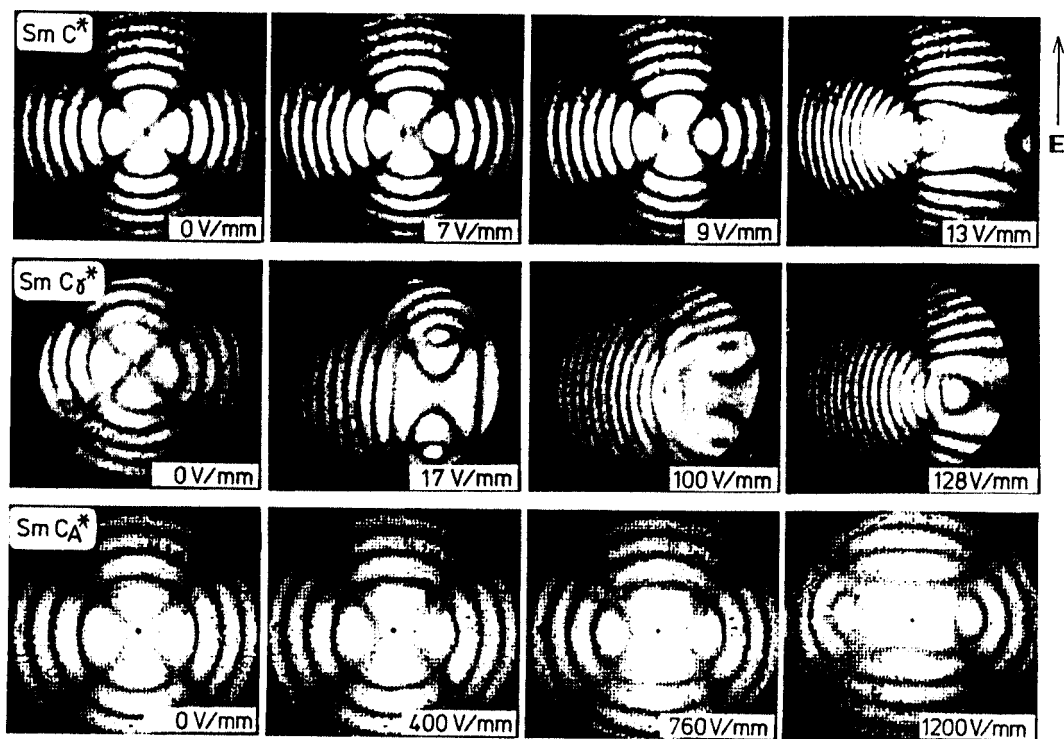


Fig. 4.1: The experimentally observed conoscopic figures in the ferro, ferri and antiferr-electric phases under several field strengths. After Ref. [15]

to obtain the conoscopic figures is $200\mu\text{m}$ as relatively thick samples are required for this purpose. They found the following characteristic changes of the conoscopic figures as a function of field in the various phases exhibited by AFLC:

1. All the tilted phases in the absence of the field give rise to a conoscopic pattern which corresponds to that of an uniaxial medium. Thus the conoscopic figures (left column of Fig. 4.1) in these cases consist of a Maltese cross with the *isogyres* parallel to the crossed analyzer and polarizer and a series of concentric circular *isochromes* (see Sec. 4.3.1 for the definition of isogyres and isochromes). This indicates that in the absence of the field, all the tilted phases have helical structures giving rise to a macroscopic uniaxial medium with optic axis parallel to the layer normal.
2. In the SmC_β^* phase, the field induced changes in the conoscopic figure are the same as those of the well known ferroelectric SmC^* phase. The uniaxial profile due to the helical structure in the absence of the field changes to a biaxial one upon application of a field and the center of the conoscopic figure shifts in a direction decided by the positive sign of polarization in this compound (in Fig. 4.1 towards right). This is because of the field induced helix unwinding and the weak biaxiality of the tilted SmC^* layers. The optic axial plane containing the two optic axes of the resulting biaxial medium is *perpendicular* to the field. The shift of the center indicates that the acute bisectrix in the medium is at an angle with respect to the layer normal.
3. The field dependence of the conoscopic figures in the ferroelectric SmC_γ^* phase is somewhat complicated. Again the uniaxial figure in the absence of the field goes over to a biaxial one upon the application of a field with the shift of the center in the same direction as in the SmC_β^* phase. But unlike in SmC_β^* phase, at low fields, the optic axial plane in this phase is *parallel* to the field which switches to the *perpendicular* direction at higher fields (see middle row of Fig. 4.1).
4. The field induced changes in the conoscopic patterns in the antiferroelectric SmC_A^* phase is also quite characteristic of this phase. The uniaxial figure under increasing field strength changes to the biaxial one with the optic axial plane *perpendicular* to the field. However, there is no significant shift of the center upto the maximum field strength of $1200\text{V}/\text{mm}$ used in the experiment.
5. The conoscopic figures obtained experimentally by Hiraoka *et al.* [14] in the SmC_α^* phase as a function of field is shown in Fig. 4.2. The characteristic changes of the conoscopic figures in this phase are similar to those in the ferroelectric SmC_γ^* phase. However, as the SmC_α^* phase appears just below the SmA phase, the tilt angle in this phase is very small and hence the shift of the center as well as the splitting of the isogyres are very small.

A detailed comparison of these experimental observations with our theoretical predictions will be taken up in Sec. 4.3.3 of this chapter. However, here we want to point out that Gorecka *et al.* [15] based on their observations particularly those in the ferroelectric SmC_γ^* phase argued that the theoretical models of xy-type based on the azimuthal degrees of freedom of the director \hat{n} within the layer could not account for the optic axial plane lying parallel to the field. Using qualitative arguments they tried to interpret their observations

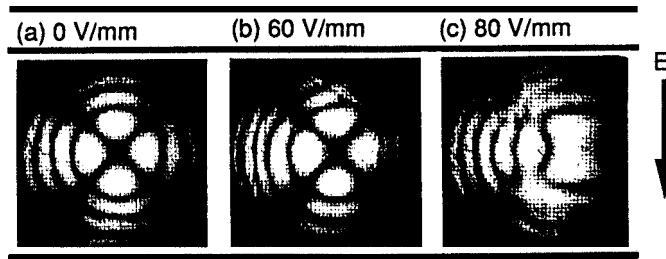


Fig. 4.2: The experimental conoscopic figures in the SmC_α^* phase. Note the optic plane change from (b) to (c). After Ref. [14].

by assuming the orientational configuration of the director \hat{n} within each layer as an Ising variable. Their observations in the ferroelectric phase are often quoted in the literature against the xy-type models of the AFLC and used in favour of other alternative models [13, 19] of Ising type. However, the xy character of the orientational order parameter in such systems is well known [31, 50] from the studies of ferroelectric SmC^* liquid crystals which is also one of the phases exhibited by AFLC. The uniaxial character of the zero field conoscopic figures in all the tilted phases exhibited by AFLC indicates that the azimuthal degrees of freedom of the director \hat{n} can not be ignored. Therefore, the assumption of the Ising character of the orientation of the director \hat{n} in each layer is questionable.

On the other hand we will show that the theoretically simulated conoscopic figures corresponding to the field free and field induced structures predicted by our xy-type model is in complete agreement with the experimental observations. Thus the conjecture [15] that the xy type model can not account for the experimentally observed conoscopic figures in the ferroelectric phase is not sustainable.

Another powerful optical technique often used to elucidate the structures of the different phases exhibited by AFLC is the ellipsometric studies on the free standing films (see Sec. 4.4.1 for a general introduction of ellipsometry). Bahr *et al.* [5, 23, 24] have performed a number of experiments on AFLC free standing films. In their experimental setup free-standing films are prepared by drawing a small amount of sample in the smectic state across a $3 \times 12 \text{ mm}^2$ rectangular hole in a 0.15 mm thick glass plate. In a free-standing film, smectic layers align parallel to the film surface and the film normal corresponds to the layer normal. The long sides of the hole are conductively coated and an electric field can be applied in the film plane. The film is maintained in a one stage oven with a temperature stability of $\approx 0.05^\circ\text{C}$. A He-Ne laser beam ($\lambda = 633 \text{ nm}$) is incident on the film at an angle of 45° with respect to the film normal and perpendicular to the aligning electric field. The light is linearly polarized with an azimuthal angle of 45° with respect to the plane of incidence, i.e., the p- and s-polarized components of the incident beam have the same phases ($A_p = A_s$) and amplitudes ($|T_p| = |T_s|$). They can measure the ellipsometric parameters $A = \Delta_p - A_s$, and $\Psi = \tan^{-1}(|T_p|/|T_s|)$ of the transmitted light. The polarization state of the incident light is described by $A = 0$ and $\Psi = 45^\circ$. After the transmission through the film, the light is elliptically polarized with a non-zero phase difference A and a value of Ψ deviating from 45° . They measured Δ_+ and Δ_- corresponding to the two polarities of the small applied electric field (-6.0 V/cm) as a

function of temperature in different phases exhibited by AFLC.

The details of their experimental observations will be presented in Sec. 4.4.3. Some of the important experimental observations in these ellipsometric studies are:

- The difference ($A_+ - \Delta_-$) in the antiferroelectric SmC_A^* phase is zero for even number of layers but nonzero for odd number of layers in the film. This clearly demonstrates that the SmC_A^* phase has almost opposite tilt directions in successive layers [5].
 - a All the sub-phases exhibited by AFLC persist even in films consisting of only 4 or 5 layers.
- A small difference between A_+ and Δ_- remains even in the SmA phase. This has been attributed to the fact that even though the interior layers are in the SmA state the surface layers may be tilted [23].
 - a They have not found the evidence for the 1:2 structure which is often proposed [8] as the structure of the ferrielectric SmC_γ^* phase. The ellipsometric parameters obtained in this phase show a non-smooth variation with temperature.
 - a In the SmC_α^* phase, they found a number of oscillations of the ellipsometric parameters A_+ and Δ_- as a function of temperature. The number of oscillations decreases as the number of layers in the film is decreased.
 - a They claimed that the aligning field applied is so small (6 V/cm) that it cannot distort the helical structure in a significant way. However, this aligning field can align the net polarization which will in general be nonzero for the finite number of layers used in the experiments.

They qualitatively argued that the oscillations seen in the SmC_α^* phase correspond to the structures given by the devil's staircase produced by the Ising picture. However, in this chapter, we will show that these ellipsometric observations can also be explained on the basis of our model.

For the sake of completeness, we have also calculated the optical rotatory power (ORP) in the different phases as a function of temperature in the absence of the field. Philip et al. [10] have performed some experiments to measure the ORP in the various phases as a function of temperature. They did not perform experiments in the ferrielectric SmC_γ^* phase as they found that even if the alignment in the higher temperature SmC_β^* phase and in the lower temperature SmC_A^* phase appear uniform under the microscope, the ferrielectric SmC_γ^* phase appears highly non-uniform and turbid with in-plane birefringence.

Due to the underlying layer structure of the smectic phases and the inhomogeneous orientation of the director \hat{n} along the layer normal, the appropriate technique to calculate the reflection or transmission properties of the medium is the Berreman's 4 x 4 matrix method. Therefore we start with a brief discussion of the basic ingredients of this method.

4.2 Berreman's 4×4 matrix method

An appropriate formalism for the computation of the parameters describing the propagation of light in an anisotropic medium stratified along one direction is the 4×4 matrix method, which was introduced by Teitler and Henvis [51] and applied to liquid crystalline systems by Berreman [52]. The method is a generalization of the Abele's 2×2 matrix method [53] applicable to a stratified isotropic medium.

For simplicity, we will assume that the medium is free of optical activity and is non-magnetic *i. e.*, $\mu = 1$. Maxwell's equations in such a medium in the absence of charges and currents ($\rho = \vec{j} = 0$) are given by

$$\vec{\nabla} \times \vec{E} = -\frac{1}{c} \frac{\partial \vec{H}}{\partial t}, \quad \vec{\nabla} \times \vec{H} = \frac{1}{c} \epsilon \frac{\partial \vec{E}}{\partial t}, \quad (4.1)$$

where $\epsilon = \epsilon(z)$ is the dielectric tensor, whose principal values are ϵ_1 , ϵ_2 and ϵ_3 . For a medium stratified along the z -direction, ϵ depends only on z . The invariance of Eqs. 4.1 under translation of time and of x , y coordinates implies that the solutions are of the following type:

$$\begin{aligned} \vec{E} &= \frac{1}{2} \vec{E}(z) e^{i(k_x x + k_y y - \omega t)} + \text{CC.}, \\ \vec{H} &= \frac{1}{2} \vec{H}(z) e^{i(k_x x + k_y y - \omega t)} + \text{CC.} \end{aligned} \quad (4.2)$$

Following Berreman, we have used the convention of $e^{-i\omega t}$ for time dependence. The equations corresponding to the $e^{i\omega t}$ convention can be obtained by replacing i by $-i$ in the appropriate expressions. By substituting 4.2 into Eq. 4.1, we obtain

$$\begin{pmatrix} 0 & -d/dz & ik_y \\ d/dz & 0 & -ik_x \\ -ik_y & ik_x & 0 \end{pmatrix} \begin{pmatrix} E_x \\ E_y \\ E_z \end{pmatrix} = i \frac{\omega}{c} \begin{pmatrix} H_x \\ H_y \\ H_z \end{pmatrix} \quad (4.3)$$

$$\begin{pmatrix} 0 & -d/dz & ik_y \\ d/dz & 0 & -ik_x \\ -ik_y & ik_x & 0 \end{pmatrix} \begin{pmatrix} E_x \\ E_y \\ E_z \end{pmatrix} = -i \frac{\omega}{c} \begin{pmatrix} \epsilon_{xz} & \\ \epsilon_{yz} & \\ \epsilon_{zx} & \epsilon_{zz} \end{pmatrix} \begin{pmatrix} E_x \\ E_y \\ E_z \end{pmatrix} \quad (4.4)$$

Here we have two sets of three equations. The last equation in each set does not contain derivatives with respect to z . Consequently, E_z and H_z can be expressed in terms of the other components as

$$H_z = \frac{c}{\omega} (k_x E_y - k_y E_x), \quad E_z = -\frac{c}{\omega} (k_x H_y - k_y H_x + \epsilon_{zx} E_x + \epsilon_{zy} E_y) / \epsilon_{zz}. \quad (4.5)$$

Eliminating H , and E , from the other four equations, we get

$$\frac{d\psi}{dz} = i \frac{\omega}{c} D(z) \psi, \quad (4.6)$$

where

$$\psi^T = (E_x, H_y, E_y, -H_x) \quad (4.7)$$

is the generalized field vector and

$$D = \begin{bmatrix} \left(-k_x \frac{\epsilon_{zx}}{\epsilon_{zz}} \right) & \left(1 - \frac{k_x^2}{\epsilon_{zz}} \right) & \left(-k_x \frac{\epsilon_{zy}}{\epsilon_{zz}} \right) & \left(-\frac{k_x k_y}{\epsilon_{zz}} \right) \\ \left(\epsilon_{xx} - \frac{\epsilon_{xz}\epsilon_{zx}}{\epsilon_{zz}} - k_y^2 \right) & \left(-k_x \frac{\epsilon_{xz}}{\epsilon_{zz}} \right) & \left(\epsilon_{xy} - \frac{\epsilon_{xz}\epsilon_{zy}}{\epsilon_{zz}} + k_x k_y \right) & \left(-k_y \frac{\epsilon_{zx}}{\epsilon_{zz}} \right) \\ \left(-k_y \frac{\epsilon_{zx}}{\epsilon_{zz}} \right) & \left(-\frac{k_y k_x}{\epsilon_{zz}} \right) & \left(-k_y \frac{\epsilon_{zy}}{\epsilon_{zz}} \right) & \left(1 - \frac{k_y^2}{\epsilon_{zz}} \right) \\ \left(\epsilon_{yx} - \frac{\epsilon_{zx}\epsilon_{yz}}{\epsilon_{zz}} + k_y k_x \right) & \left(-k_x \frac{\epsilon_{yz}}{\epsilon_{zz}} \right) & \left(\epsilon_{yy} - \frac{\epsilon_{yz}\epsilon_{zy}}{\epsilon_{zz}} - k_x^2 \right) & \left(-k_y \frac{\epsilon_{yz}}{\epsilon_{zz}} \right) \end{bmatrix} \quad (4.8)$$

is the 4x4 differential propagation matrix of the medium. Note that not all the elements of the differential propagation matrix D are independent. It has been proved by Eidner *et al.* [54] that D has only 10 independent elements with the following symmetry:

$$D_{11} = D_{22}^*, D_{33} = D_{44}^*, D_{41} = D_{23}^*, D_{32} = D_{14}^*, D_{42} = D_{13}^*, D_{31} = D_{24}^*.$$

The matrix $D(z)$ depends mainly on the components of the dielectric tensor and therefore on the director configuration within the liquid crystal. The solution of Eq 4.6 can be written using a 4 x 4 transfer matrix F as

$$\psi(z_2) = F(z_1, h)\psi(z_1), \quad (4.9)$$

where $h = z_2 - z_1$. All relevant optical parameters can be computed from F . Therefore the main problem of the 4 x 4 matrix technique is to determine the matrix F which relates the tangential component of the electric and magnetic fields at z_1 to those at z_2 .

When the medium is homogeneous (*i.e.*, D is independent of z) over a finite distance h ($= z_2 - z_1$) along the z -axis, Eq. 4.6 may be integrated to give

$$\psi(z+h) = P(h)\psi(z) \quad (4.10)$$

and a closed form expression for P can always be found. To see this, first note that there will be four periodic solutions of Eq. 4.6, which are of the form

$$\psi_j(z+h) = e^{iq_j h} \psi_j(z). \quad (4.11)$$

The four eigenvalues q_j may be obtained by substituting Eq. 4.11 into Eq. 4.6 and then solving the quartic polynomial equation in q resulting from the determinant in the secular equation

$$\text{Det}(k_o D - qI) = 0 \quad (4.12)$$

where $k_o = \omega/c$ and I is the 4 x 4 identity matrix. The corresponding eigenvectors ψ_j can then be found by three of the four simultaneous equations represented by the matrix equation

$$k_o D \psi_j = q_j \psi_j. \quad (4.13)$$

Now an expression for $P(h)$ can be written as

$$P(h) = \Psi K(h) \Psi^{-1}. \quad (4.14)$$

where Ψ is a 4 x 4 matrix formed from the elements ψ_{ij} of the four eigen vectors and $K(h)$ is a 4 x 4 diagonal matrix with elements

$$K_{jj}(h) = \exp(iq_j h). \quad (4.15)$$

An alternative expression for \mathbf{P} is obtained by simply expanding the exponential function in powers of the matrix \mathbf{D} as

$$P = \exp(-ik_o Dh) = I - i \frac{k_o h}{1!} D - \frac{(k_o h)^2}{2!} D^2 + \dots \quad (4.16)$$

From Eq. 4.16, one useful symmetry of $P(h)$ is

$$P(mh) = [P(h)]^m, \quad (4.17)$$

where m is any positive or negative integer or zero.

For a medium in which the dielectric tensor depends on z , in general an analytic solution of Eq. 4.6 can not be found. However, a numerical solution can always be found by assuming the medium as a stack of layers of thickness h along the z -axis and the dielectric tensor ϵ within each layer as homogeneous. When ϵ varies continuously along z , the above approximation can be made better by choosing h sufficiently small. In smectic liquid crystals, the medium can be well approximated as stacks of layers along the z -axis and the method can be applied efficiently.

With this approximation, let the matrix $P_i(h)$ denote the transfer matrix of the i -th layer, which relates the generalized field vector ψ of the i -th layer to that of the $(i+1)$ th layer. Because Eq. 4.10 applies to each layer, we may use the equation repeatedly to obtain the transfer matrix $F(i, n)$ which relates the vectors ψ of i th and $(i+n)$ th layers as:

$$F(i, n) = P_{i+n}(h)P_{i+n-1}(h) \cdots P_{i+1}(h)P_i(h). \quad (4.18)$$

If ϵ is a periodic function of x , Eq. 4.18 needs to be used over only one period or cycle and the transfer matrix corresponding to m such cycles can be obtained by taking the m th power of the transfer matrix for a single period. In the above exposition of the Berreman's 4×4 matrix technique, we have assumed that the medium is non-magnetic *i.e.*, $\mu = 1$ and free of optical activity. Since the molecules are chiral in the AFLC, the medium is in principle not free of optical activity. However, the optical rotation produced by the optical activity of the medium is far less compared to that produced by the form of the director field. Thus this assumption is often used in the discussion of optical properties of other chiral liquid crystalline phases *viz.* cholesteric and SmC* phases. Indeed, the inclusion of the weak optical activity of the medium will not change appreciably the optical properties investigated in this chapter and can be neglected as a first approximation. However, in a more general theory the above assumptions can be relaxed. The description of this general case can be found in the original treatment by Berreman [52].

4.3 Generating conoscopic figures

4.3.1 What is conoscopy?

The examination of a medium in a parallel beam of light between crossed polarizers reveals its optical character only along one direction. Very important additional information may be obtained by passing a strongly corivergent beam of light through the medium to examine its optical properties in many directions at the same time. The observation

between crossed polarizers in this case does not focus on the image of the object (object image), but on another optical image formed at the principal focus of the objective by the strongly convergent beam of light. This image is variously called, the *direction image* (as opposed to object image), the *conoscopic figure* or the *interference figure*.

Since the rays of the convergent beam passing through the anisotropic sample are not parallel, the path followed by different rays will be longer the greater their angle of incidence. Moreover, these rays will be normal to different sections of the refractive indicatrix. It therefore follows that the interference figure from a flat slab with parallel sides made of such an anisotropic sample will not show a uniform interference colour as it does when it is viewed in parallel light between crossed polarizers. A series of curved interference bands, which are coloured in white light and bright and dark in monochromatic light, will be seen. These interference bands are systematically arranged around the optic axis (or axes) and are called *isochromes*. In addition to these isochromes there are dark "brushes" or *isogyres*, the shape of which is determined by the position of those points on the interference figure, where the plane of vibration of the rays are parallel or perpendicular to the polarizer (see Fig. 4.1).

By studying the conoscopic figure or the interference figure of the sample, the following optical characteristics may be determined:

- In general
 1. Isotropic substances may be differentiated from the sections of an anisotropic sample normal to the optic axis.
 2. Anisotropic substances may be classified optically as belonging to the uniaxial or biaxial class.
 3. For uniaxial samples, the positive or negative sign of the uniaxiality of the substance may be determined.
 4. If the thickness of the sample is known, an estimate of the birefringence may be made.
- In a biaxial medium
 1. The direction of the *optic axial plane i.e.*, the plane containing the two optic axes of the medium may be found.
 2. The angle between the two optic axes or the *optic axial angle* may be measured.
 3. The dispersion of the optic axes may be studied.

4.3.2 Simulating conoscopic figures for AFLC

We now apply Berreman's 4 x 4 matrix method described in Sec. 4.2 to calculate the conoscopic figures produced by a cell containing *homeotropically* aligned AFLC. It is assumed that the polarizer and (crossed) analyzer are perfect polarizers for normally incident light and the condenser and objective lens systems are free from spherical and other aberrations for the monochromatic light used. Fig. 4.3 shows the experimental geometry and the coordinate system used in the conoscopic calculations. A parallel beam of light passing

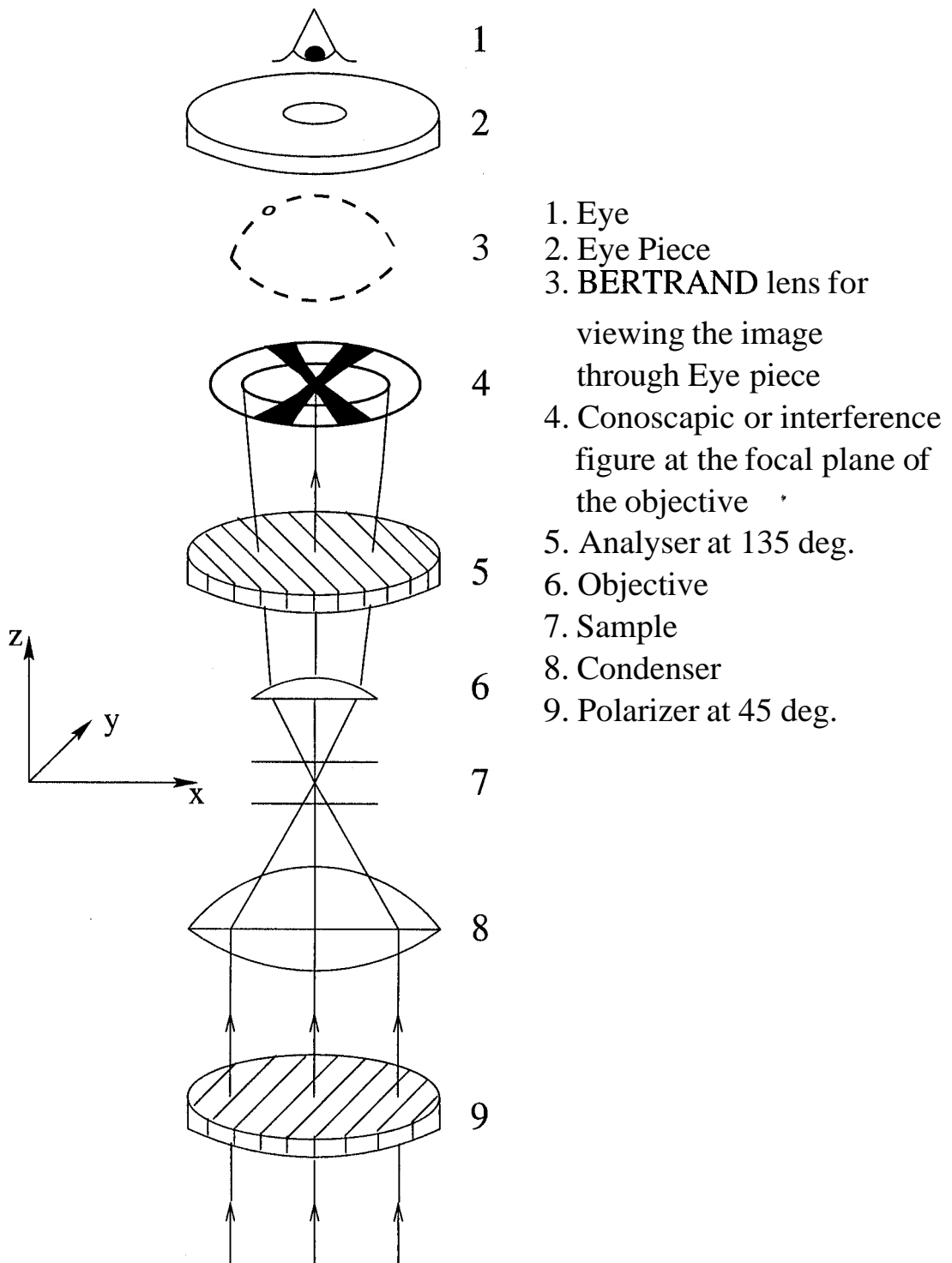


Fig. 4.3: A schematic diagram of a general experimental arrangement for observing the conoscopic figures. The angle of the polarizer and analyzer axes are measured with respect to the x-axis.

through the polarizer aligned at an angle of 45° with respect to the x-axis is made convergent and focused onto the homeotropically oriented AFLC cell by the condenser. The transmitted beam from the sample cell then passes through the objective lens system and the crossed analyzer to form the required conoscopic figure. For simplicity we assume that each ray of the convergent beam from the condenser can be represented as a plane wave with the wave vector \vec{k} defined as

$$\vec{k} = k(\sin A \cos C, \sin A \sin C, \cos A)$$

where A and C are the polar and azimuthal angles of \vec{k} measured with respect to the z-axis and x-axis respectively. For each such propagation direction, we calculate the transmitted intensity by Berreman's 4 x 4 matrix technique. In our calculation the azimuthal angle C is taken to vary from 0 to 2π in steps of $\pi/18$ whereas the polar angle A varies from 0 to $\pi/4$ in steps of $\pi/90$. Though smaller step sizes improve the quality of the conoscopic figures the calculations become time consuming. We found this discretization of A and C are optimum without losing the clarity of the figures.

To calculate the transmitted intensity for a given direction (A,C) consider an AFLC cell consisting of N flat layers with the layer normal perpendicular to the bounding glass plates (*i.e.*, along z-axis). Since each of these smectic layers with tilted molecules is optically biaxial, the dielectric tensor ϵ' in the principal coordinate system $x'y'z'$ can be written as

$$\epsilon' = \begin{bmatrix} \epsilon_1 & 0 & 0 \\ 0 & \epsilon_2 & 0 \\ 0 & 0 & \epsilon_3 \end{bmatrix} \quad (4.19)$$

where z'-axis is assumed to be parallel to the director \hat{n} and y'-axis is along the C_2 axis ($\hat{n} \times \hat{k}$) as shown in Fig. 2.1. We define the dielectric anisotropy $\Delta\epsilon$ and the dielectric biaxiality $\delta\epsilon$ as

$$\Delta\epsilon = \epsilon_3 - \epsilon_1; \quad \delta\epsilon = \epsilon_2 - \epsilon_1. \quad (4.20)$$

The dielectric tensor ϵ in the lab frame (xyz system) can be obtained from ϵ' in the principal coordinate system ($x'y'z'$ frame) of the layer by transforming the latter as

$$\epsilon = T\epsilon'T^{-1}, \quad (4.21)$$

where T is the transformation matrix from the principal coordinate system ($x'y'z'$) to lab frame (xyz). If the orientation of the director \hat{n} in the lab frame is given by

$$\hat{n} = (\sin\theta \cos\phi, \sin\theta \sin\phi, \cos\theta)$$

where the azimuthal angle ϕ of the director \hat{n} is measured from the x-axis, the transformation matrix T takes the form

$$T = \begin{bmatrix} \cos\theta \cos\phi & -\sin\phi & \sin\theta \cos\phi \\ \cos\theta \sin\phi & \cos\phi & \sin\theta \sin\phi \\ -\sin\theta & 0 & \cos\theta \end{bmatrix} \quad (4.22)$$

Using T from Eq. 4.22 and ϵ' from Eq. 4.19 in eq. 4.21, the dielectric tensor ϵ in the lab frame is given by the symmetric matrix

$$\epsilon = \begin{bmatrix} \epsilon_{xx} & \epsilon_{xy} & \epsilon_{xz} \\ \epsilon_{yx} & \epsilon_{yy} & \epsilon_{yz} \\ \epsilon_{zx} & \epsilon_{zy} & \epsilon_{zz} \end{bmatrix} \quad (4.23)$$

where

$$\begin{aligned}
\epsilon_{xx} &= \epsilon_1 + \Delta\epsilon \sin^2 \theta \cos^2 \phi + \delta\epsilon \sin^2 \phi, \\
\epsilon_{xy} &= \epsilon_{yx} = \Delta\epsilon \sin^2 \theta \sin \phi \cos \phi - \delta\epsilon \sin \phi \cos \phi, \\
\epsilon_{xz} &= \epsilon_{zx} = \Delta\epsilon \sin \theta \cos \theta \cos \phi, \\
\epsilon_{yy} &= \epsilon_1 + \Delta\epsilon \sin^2 \theta \sin^2 \phi + \delta\epsilon \cos^2 \phi, \\
\epsilon_{yz} &= \epsilon_{zy} = \Delta\epsilon \sin \theta \cos \theta \sin \phi, \\
\epsilon_{zz} &= \epsilon_1 + \Delta\epsilon \cos^2 \theta.
\end{aligned}$$

In our calculations we have assumed that the dielectric anisotropy $\Delta\epsilon = 0.64$, the dielectric biaxiality $\delta\epsilon = 0.009$ and $\epsilon_1 = 2.25$ [15].

If the director configuration of each layer is known, one can construct the differential propagation matrix D for each layer from Eq. 4.8 using the dielectric tensor in Eq.4.23 and k_x , k_y as

$$k_x = n_1 \sin A \cos C, \quad k_y = n_1 \sin A \sin C. \quad (4.24)$$

where n_1 is the refractive index of the entrance medium. Therefore the transfer matrix P for each layer can be computed as described in Sec. 4.2. We calculate P for a given layer by exponentiating the matrix D as in Eq. 4.16 using MATLAB. In calculating the matrix P for each layer, we use the thickness of the layer as $d \cos \theta$ where d is assumed to be 40\AA . This process is repeated and the resulting P matrices are multiplied as in Eq. 4.18 to get the final transfer matrix $F(1, N)$ for the entire N layer system.

Then the vector ψ_1 at the first surface is related to the vector ψ_N at the second surface by the matrix equation

$$\psi_N = F(1, N)\psi_1. \quad (4.25)$$

The field vector at the first surface is made up of two parts with the incident- and reflected-wave contributions

$$\psi_1 = \psi_i + \psi_r. \quad (4.26)$$

The field at the second surface matches only a single transmitted wave field

$$\psi_N = \psi_t. \quad (4.27)$$

If the entrance and exit media are non-absorbing and isotropic, only two electric field components are needed to complete the definition of the incident wave, since the magnetic field components can be expressed in terms of the electric field components in isotropic media. Therefore we write

$$\psi_i = \begin{bmatrix} E_x \\ a_2 E_x + a_1 E_y \\ E_y \\ a_1 E_x + a_3 E_y \end{bmatrix}, \quad \psi_r = \begin{bmatrix} R_x \\ -(a_2 R_x + a_1 R_y) \\ R_y \\ -(a_1 R_x + a_3 R_y) \end{bmatrix}, \quad \psi_t = \begin{bmatrix} T_x \\ a'_2 T_x + a'_1 T_y \\ T_y \\ a'_1 T_x + a'_3 T_y \end{bmatrix} \quad (4.28)$$

where

$$\begin{aligned}
a_1 &= n_1 \tan A \sin A \sin C \cos C, \\
a_2 &= n_1 \tan A \sin A \cos A \cos^2 C, \\
a_3 &= n_1 \tan A \sin A \cos A \sin^2 C.
\end{aligned} \quad (4.29)$$

SECTION 4.3

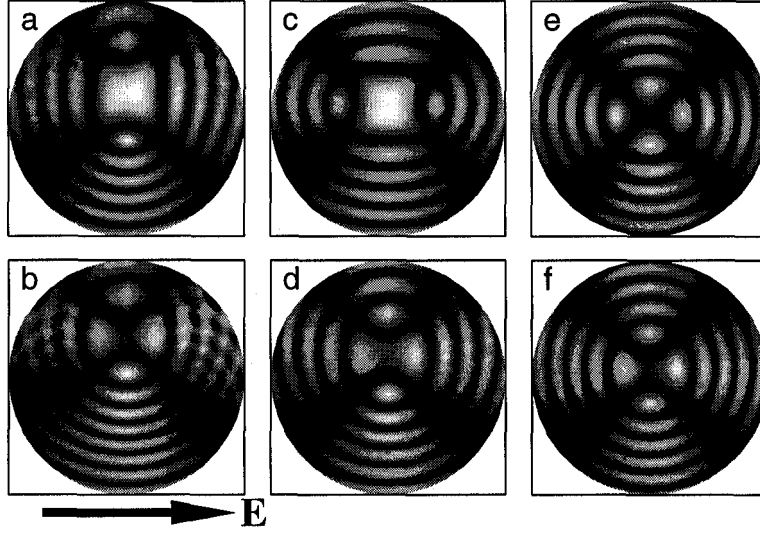


Fig. 4.4: Theoretically simulated conoscopic figures in the different phases at different fields. Left column: SmC_A^* phase (a) $E_{eff} = 5.0$ (b) $E_{eff} = 7.1$; middle column: FI_L phase (c) $E_{eff} = 2.0$ (d) $E_{eff} = 3.0$; right column: SmC_α^* phase (e) $E_{eff} = 1.6$ (f) $E_{eff} = 4.4$, where $E_{eff} = \chi\lambda E \times 10^4$. Note the optic axial plane in (c) and (e) is orthogonal to that in other figures. At higher fields (b),(d) and (f) the better unwinding causes the shift of the center towards the top.

A similar definition of a'_1 , a'_2 and a'_3 can be obtained from Eq. 4.29 by replacing the refractive index n_1 of the entrance medium with the refractive index n_2 of the exit medium. In our calculation both the entrance and exit media are taken as glass with refractive indices $n_1 = n_2 = 1.5$.

Now substituting ψ_1 and ψ_N from Eq. 4.26, Eq. 4.27 and Eq. 4.28 in Eq. 4.25, we get four linear equations for T_x , T_y , R_x , and R_y . Therefore, the transmitted electric components T_x , T_y , and reflected electric components R_x , R_y can be obtained by solving these linear equations.

4.3.3 Comparison with experiments

The simulated conoscopic figures in different phases are shown in Fig. 4.4. For this purpose the equilibrium configurations of the N-layer stack are found by the procedure discussed in Chapter 3. To generate the patterns the transmitted intensities are mapped to a plane using 128 level grey shade by MATLAB routines. Since in the absence of electric field all the tilted phases have helicoidal structure, the medium is optically uniaxial. Therefore the conoscopic figure in these uniaxial phases consists of a Maltese cross with the isogyres along the polarizer and analyzer directions and a series of concentric circular isochromes. These are not shown in Fig. 4.4. But in the presence of the electric field, the uniform helical structure is distorted and the medium acquires biaxial characteristics. In the

SmC_A^* phase, at intermediate fields, the commensurate $1/2$ structure is stable and gives rise to the conoscopic figure as shown in Fig. 4.4a. The conoscopic figure in this phase corresponds to that of a biaxial medium with the optic axial plane perpendicular to the field. At higher fields, all the layers tilt in the same direction in the unwound ferroelectric phase giving rise to the conoscopic figure shown in Fig. 4.4b.

In the ferroelectric SmC_β^* phase as the field is increased, due to the unwinding of the helix, the conoscopic figure shows the characteristics of a biaxial medium with the optic axial plane perpendicular to the electric field. In the ferroelectric FI_L phase at intermediate fields a $2/3$ commensurate structure is stable (see Fig. 3.8b) and the conoscopic figure (Fig. 4.4c) in this phase corresponds to that of a biaxial medium with the optic axial plane *parallel* to the electric field. At higher fields this phase reenters to the soliton lattice structure and gives rise to a conoscopic figure with the optic axial plane orthogonal to \vec{E} as shown in Fig. 4.4d. This trend is in close agreement with that seen in experiments in the ferroelectric SmC_γ^* phase (see Fig. 4.1). In the SmC_α^* phase the field induced $2/4$ structure (see Fig. 3.8c) gives rise to a small splitting in the plane containing \vec{E} (Fig. 4.4e) indicating biaxiality. At higher fields, the unwound structure again produces a splitting in the orthogonal plane as shown in Fig. 4.4f. In this case, as the tilt angle is very small, the shift of the center as well as the biaxiality of the medium are relatively small. We see that the patterns shown in Fig. 4.4 compare extremely well with the experimental results on the relevant phases shown in Fig. 4.1 and 4.2.

Here we like to emphasize again the following experimental observations:

1. The apparent tilt angle in the absence of field is zero in all the tilted sub-phases.
2. There is a plateau at one third of the tilt angle for intermediate fields in the ferroelectric phase (see Fig. 3.10).
3. The conoscopic figures in all the tilted phases in the absence of a field corresponds to that of an uniaxial medium (Fig. 4.1).
4. For intermediate fields, the conoscopic figures in the ferroelectric phase corresponds to that of a biaxial medium with the optic axial plane *parallel* to *i.e.*, containing the field (Fig. 4.1).

Indeed these experimental observations can be explained naturally from our model. Both the observations (1) & (3) is due to the helicoidal structure of the ferroelectric phase predicted by our model in the absence of a field. On the other hand the observations (2) & (4) arise due to the field *induced* $2/3$ structure in the ferroelectric phase predicted by our model. This implies that the $2/3$ structure, which is similar to the 1:2 ($\sqrt{} \setminus \dots$) structure often proposed for ferroelectric phase is *field induced* but does not occur in the absence of field. Thus, the claim made by Gorecka *et al.* that the xy-type model can not explain the observed conoscopic figures in the ferroelectric phase is not sustainable.

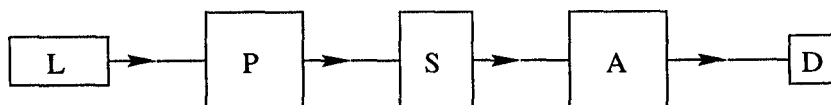


Fig. 4.5: An operational diagram of a general ellipsometer arrangement. L, P, S, A and D represent a light source, controlled polarizer, optical system under investigation, variable polarization analyzer and the photo-detector respectively.

4.4 Ellipsometry

4.4.1 General introduction

Ellipsometry is an optical technique for the characterization of, and observation of events at, an interface between two media or a film and is based on exploiting the polarization transformation that occurs as a beam of polarized light is reflected from or transmitted through the interface or the film [55]. Although measurement of the state of polarization of a light wave is important in its own right, ellipsometry is generally conducted in order to obtain information about an optical system that modifies the state of polarization. In the general scheme of ellipsometry, a polarized "probe" light beam is allowed to interact with an optical system under investigation. This interaction changes the state of polarization of the wave. The ellipsometric study consists of measurement of the initial and the final states of polarization of the wave as a function of external parameters that control the properties of the optical system under investigation and/or as a function of initial state of polarization of the probing light wave.

An operational diagram of a general ellipsometer arrangement is shown in Fig. 4.5. A well collimated monochromatic or quasi-monochromatic beam from a suitable source (L) is passed through a variable polarizer (P) to produce light of known polarization. This light beam interacts with the optical system (S) under study and its polarization is modified. The modified state of polarization at the output of the system is measured (analyzed) by a variable polarization analyzer (A) followed by a photo detector (D).

Assuming the optical system to be investigated as non-absorbing and the interaction between the light wave and the optical system is linear, the optical system can change the state of polarization of the probe wave through one or a combination of the following basic processes:

1. Reflection or Refraction: When a light wave is reflected or refracted at the interface between two dissimilar media, the state of polarization is changed abruptly. Such a change occurs due to the difference in the Fresnel reflection or transmission coefficients for the two linear polarizations parallel (p) and perpendicular(s) to the plane of incidence.
2. Transmission : The change of state of polarization of light as it traverses through a medium which exhibits optical anisotropy.
3. Scattering: This is caused by the spatial inhomogeneity of the refractive index of the medium with the wave vector corresponding to this inhomogeneity comparable to

the wavelength of light used. In contrast with the reflection and transmission modes which do not significantly affect the collimation of the beam, scattering is usually accompanied by a redistribution of the scattered energy over a wide range of solid angles.

Depending upon the prevalent mode of interaction that modifies the state of polarization of light, we may distinguish between three types of ellipsometry (i) Reflection or surface ellipsometry (ii) Transmission ellipsometry and (iii) Scattering ellipsometry.

4.4.2 Calculation of ellipsometric parameters for AFLC thin films

To test the validity of the predictions of our model, we have calculated the ellipsometric parameters A_+ and Δ_- as a function of temperature to compare with the experimental ones carried out by Bahr *et al.* [5, 23, 24] (see Sec. 4.1). To calculate these ellipsometric parameters we assume that the electric field applied ($\sim 6V/cm$) is so small that it can not distort the helical structures of the director \hat{n} . In fact it is claimed by Bahr *et al.* [23] that the electric field applied in their experiments is three orders magnitude lower than the field required to induce the transition from the antiferroelectric to the ferroelectric phase. However, this small field can align the net polarization \vec{P} of the entire stack of layers. Note that the net polarization \vec{P} is in general non-zero for the finite number of layers used in these experiments. As in the experiments, the wave length of the light used in the calculations is $632.8nm$ corresponding to a He-Ne laser beam and the entrance and exit media are assumed to be air with the refractive index $n_1 = n_2 = 1.0$. Further, some of the experiments have been carried out on the compound 12F1M7 for which we do not know the various material parameters required for the calculations. Thus we have used the same material parameters used in simulating the conoscopic figures. In particular the thickness of the smectic layers in the SmA phase is assumed to be 40\AA . With these assumptions, the calculations of the ellipsometric parameters A_+ and Δ_- for an N layer system proceed as follows:

1. For a given temperature, the minimum energy configuration of the N layer system is found (see Sec. 2.4.3).
2. The direction of the net polarization \vec{P} of the N layers system is then found by vectorially adding the 2-d polarizations \vec{P}_i of all the layers.
3. As the net polarization \vec{P} aligns along the field, the light is chosen to be incident on the film in a plane perpendicular to \vec{P} and at an angle of incidence of 45° (-45°) with respect to the film normal. The light is linearly polarized with the plane of polarization making an angle 45° with respect to the plane of incidence. Berreman's 4×4 matrix technique as described in Sec. 4.2 is used for the propagation of the light through the film. The ellipsometric parameters Δ_+ (Δ_-) of the transmitted beam corresponding to the two directions of propagation 45° (-45°) with respect to the film normal are then calculated.

The above procedure is repeated for different temperatures. Thus the calculation in this case is somewhat simpler than in Sec. 4.3.2 as we have to calculate the propagation prop-

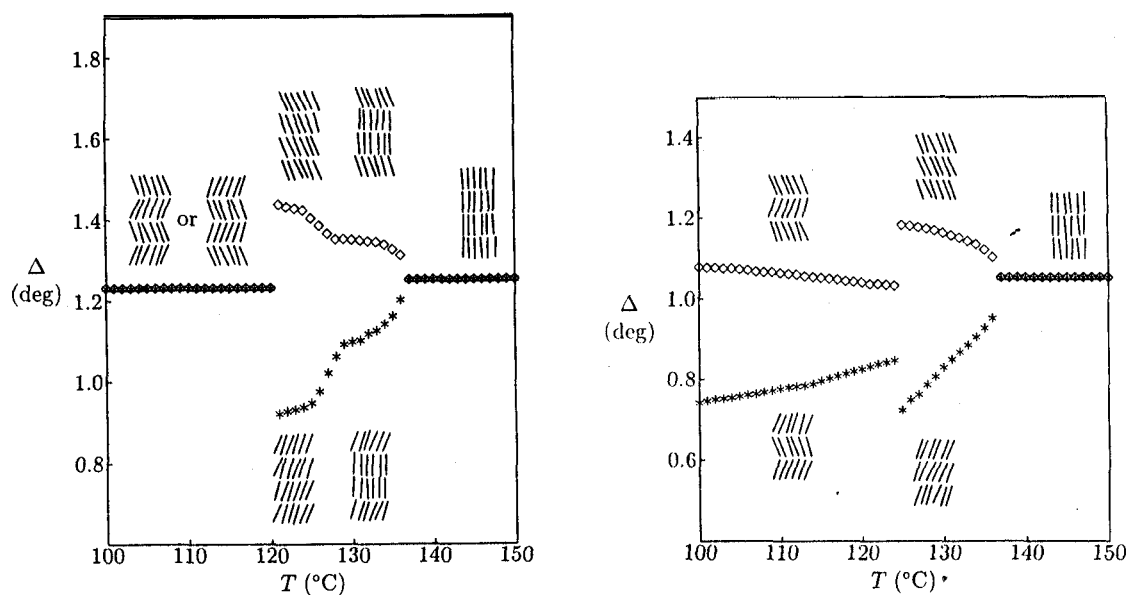


Fig. 4.6: Temperature dependences of the ellipsometric parameters A_+ and Δ_- for 4-layer and 3-layer films of MHPOBC (8:2 mixture of R and S enantiomers). After Ref. [5].

erties only for two directions. The results obtained in the various phases are described below.

4.4.3 Comparison with experiments

As mentioned in Sec. 4.1, to investigate the structure of the SmC_A^* phase, Bahr *et al.* [5] carried out ellipsometric studies on the sample consisting of 8:2 mixture of R and S enantiomers of the prototype compound MHPOBC. The mixture possesses the following bulk phase sequence: SmC_A^* -114° C- SmC_β^* -120° C- SmA -150° C-Isotropic. The temperature dependence of the ellipsometric parameters A_+ and Δ_- as obtained by them for 4-layer and 3-layer films are shown in Fig. 4.6. For temperatures above 136° C, the A values are constant and the difference between Δ_+ and Δ_- is zero as expected in the SmA phase. At 136° C the transition to the tilted layers takes place, giving rise to $A_+ - \Delta_- \neq 0$. For the 4-layer case, the tilt process seems to take place in two steps: first at 136° C only the two surface layers tilt while the interior layers remain un-tilted. Then at 127° C the remaining two interior layers also tilt. On cooling further, below 120° C, the difference between A_+ and Δ_- vanishes again as expected in the SmC_A^* phase of the film consisting of an even number of layers. The temperature variation of A values in the 3-layer case is similar to that of 4-layer film except for the fact that in the SmC_β^* phase all the layers tilt simultaneously and in the SmC_A^* phase the difference between the A_+ and A_- is non zero due to the presence of an odd number of layers. They have also studied a 2-layer film in which they found the difference between the A_+ and Δ_- in the SmC_A^* phase is again zero.

The above experimental observations clearly indicate that the bulk phase sequence

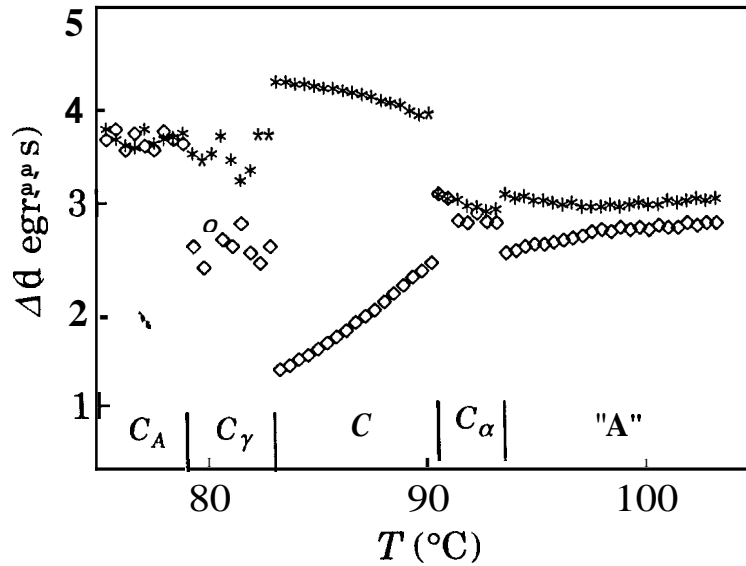


Fig. 4.7: Experimental temperature dependence of A_+ and Δ_- in the different phases for a 20-layer film of 12F1M7. After Ref. [23].

persists even for 4,3 and 2 -layer films and in the SmC_A^* phase, the alternation of the tilt direction occur in *successive* layers. Thus the periodicity of the *unwound* SmC_A^* phase is over two molecular layers. This has also been confirmed earlier by Galerne *et al.* [4] for the compound MHTAC.

In other studies Bahr *et al.* [23, 24] investigated the temperature dependence of the ellipsometric parameters of the compound 12F1M7. The compound 12F1M7 exhibits, in addition to the paraelectric SmA , ferroelectric SmC_β^* and antiferroelectric SmC_A^* phase, also the ferrielectric SmC_γ^* and the SmC_α^* phases. The temperature dependences of the A values in the various phases for different film thicknesses are shown in Fig. 4.7. For this compound, they found that the difference ($A_+ - \Delta_-$) is nonzero (see Fig. 4.7) throughout the range of stability of the SmA phase implying that the surface layers are tilted in the whole range of stability of the SmA phase. In the ferrielectric SmC_γ^* phase, there exists a considerable scattering of the A values as can be seen from the Fig. 4.7 and they did not find evidence for the 1:2 structure in the SmC_γ^* phase. In the SmA , SmC_β^* and SmC_A^* phases the variation of the A values are similar to the case of the compound MHPOBC as described earlier.

In the SmC_α^* phase, they found a number of oscillations in the A values as a function of temperature. The temperature variations of A_+ and Δ_- for a 122-layer thick film by Bahr *et al.* [24] are shown in Fig. 4.8. For the 122 layer thick film there are 4 regions in the stability range of SmC_α^* phase where the difference ($A_+ - \Delta_-$) is zero. They qualitatively interpreted these oscillations as alternating sequences of antiferroelectric and ferrielectric phases given by the Ising model first developed by Bak *et al.* [38]. As we have described in Sec. 2.3, this model was invoked for AFLC system by Takanishi *et al.* [13].

For a quantitative comparison of the above experimental observations with the theoretical predictions one should take into account in the theory the well known fact that

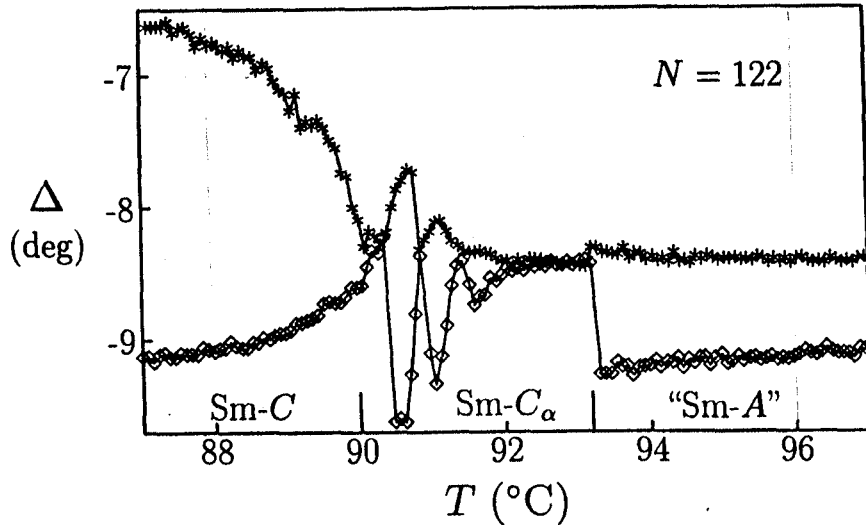


Fig. 4.8: Temperature dependence of A_+ and Δ_- in the SmA , SmC_α^* and SmC_β^* phases for a 122-layer thick film of the compound M12F1. After Ref. [24].

the surface layers in a free-standing film tilt even at 20 to 30° C above the transition temperature at which the bulk layers tilt. Moreover, even in the tilted smectic phases the surface layers have in general a different tilt angle compared to that of the bulk. Therefore, these surface layers will contribute differently to the ellipsometric parameters than the bulk layers. Further, the actual values of the material parameters of the compounds used in the experiments are not known to us. Therefore, our simple minded calculations which neglect these factors can not yield results which can be quantitatively compared with the experimental observations.

The calculated temperature variations of the ellipsometric parameters A_+ and Δ_- in the different phases for different thicknesses of the film are shown in Fig. 4.9. It is clear from Fig. 4.9 that there is a symmetry in the theoretical temperature variations of A_+ and Δ_- unlike in the experiments. This asymmetric variation of A_+ and Δ_- in the experimental observation can arise from the nucleation of defects when the aligning field is reversed as pointed out by Bahr *et al.* [23]. In spite of these differences, we see that in the SmC_α^* phase and in the high temperature region of the SmC_β^* phase there are a number of oscillations of A_+ and Δ_- as seen experimentally. The points where the difference ($A_+ - A_-$) vanishes correspond to those temperatures at which the helical pitch of the sample is such that the net polarization of the N-layer film is zero. As the variation of pitch according to our model is very sensitive to temperature in the SmC_α^* phase and the high temperature region of the SmC_β^* and also in the ferroelectric phases, these oscillations of the A values naturally arise in these phases. Moreover the number oscillations decreases as the number of layers is reduced as seen experimentally. In the SmC_β^* phase where the pitch is relatively large, A_+ and Δ_- separate out giving rise to the large difference between them as observed experimentally. In the SmC_A^* phase, pitch varies relatively slowly with temperature and gives rise to the A values which are almost equal again as seen experimentally.

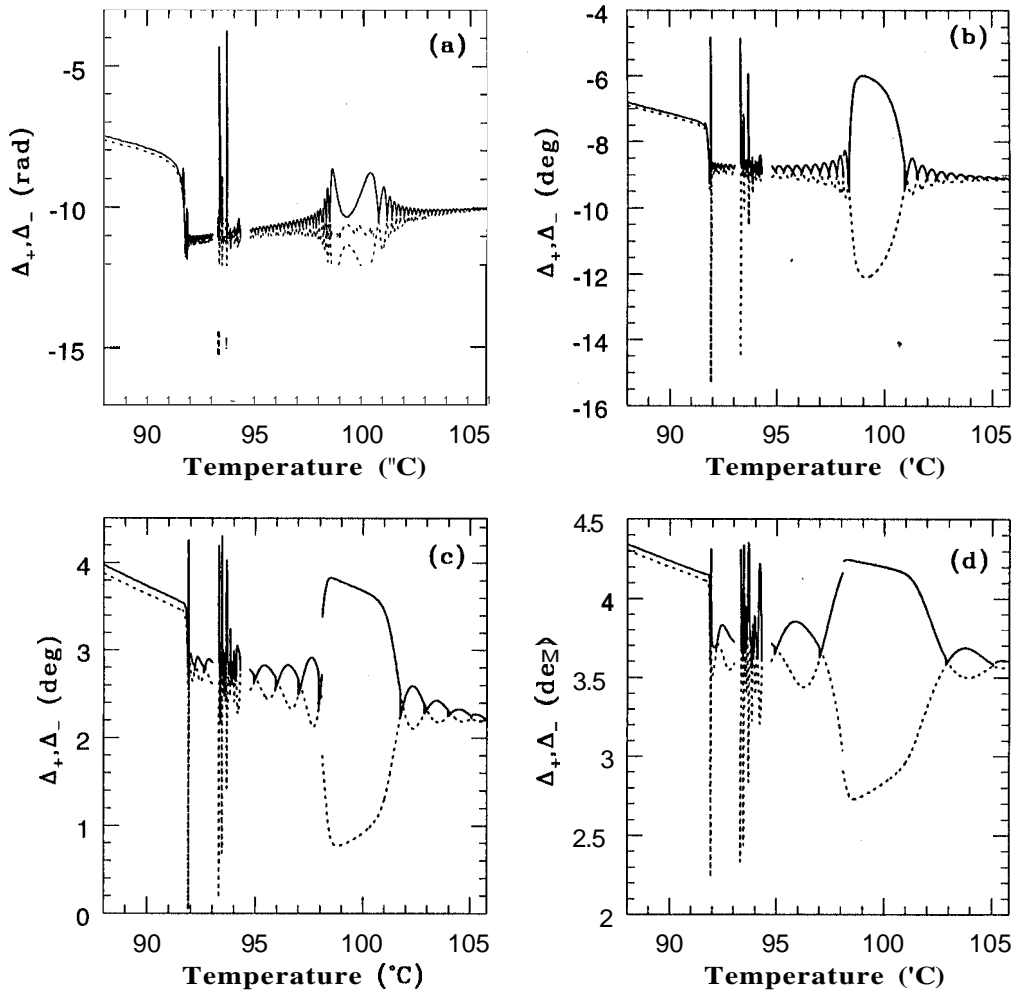


Fig. 4.9: The temperature variations of the theoretically calculated ellipsometric parameters in the different phases for (a) 122-layer, (b) 50-layer, (c) 20-layer and (d) 10-layer thick free-standing films of AFLC. The solid and dashed lines correspond to Δ_- and Δ_+ respectively.

As pointed out by Bahr *et al.* [23] they do not find any evidence for the 1:2 structure of the ferroelectric phase, which corroborates the point we made earlier that the 1:2 ($//\backslash\cdots$) is not a zero field structure. Further according to the ANNNI type models proposed for this system (see Sec. 2.3), we expect a large range of stability for the $\langle 22 \rangle$ ($//\backslash\cdots$) antiferroelectric structure. If this were true, we could expect in the 20-layer thick film (Fig. 4.7) a wide range of temperatures in the ferroelectric phase with a zero difference between the \mathbf{A} values corresponding to the $\langle 22 \rangle$ ($//\backslash\cdots$) structure. But the experimental observations (Fig. 4.7) does not give any indication of such a trend. This again implies that the ANNNI type models proposed for the antiferroelectric liquid crystal may be appropriate.

On the other hand, our model predicts sharp variations of the ellipsometric parameters in the ferroelectric range and can easily account for the scatter in the ellipsometric data. Thus sharp variation of the ellipsometric parameters with temperature arise from the large variations of $\delta\phi$ with temperature in our model.

4.5 Optical rotatory power

Another method often used to study chiral media is to measure the optical rotatory power of the sample. An incident linearly polarized plane wave after passing through the sample along the helical axis of the AFLC becomes in general elliptically polarized. The optical rotatory power (ORP) is defined as the rotation per unit length of the major axis of the polarization ellipse measured with respect to the polarization direction of the incident beam. In optically active liquid crystals, such as cholesterics and chiral smectics, optical rotation is much stronger than that of isotropic optically active liquids consisting of chiral molecules. The huge optical rotation of these liquid crystals is due to the characteristic helical structures in these phases. Therefore, optical rotatory power (ORP) measurements provide information about the helical structures in these phases.

For the sake of completeness, We have calculated the ORP in different phases by Berreman's 4×4 matrix technique. The temperature variation of the ORP in the different phases is shown in Fig. 4.10. From the figure we see that in the SmC_β^* phase there is two anomalous inversions of the ORP. These arise because the wave length of the light used in our calculation falls inside the selective reflection band of the sample due to the temperature variation of the pitch. This type of double inversion has been seen in the experiments by Furue *et al.* [56]. However, as we have mentioned earlier, Philip *et al.* [10] pointed out that the alignment of the sample in the ferroelectric phase is highly turbid and reliable measurements of ORP can not be made in this phase. Due to the lack of experimental results a detailed comparison with the calculations of ORP can not be made.

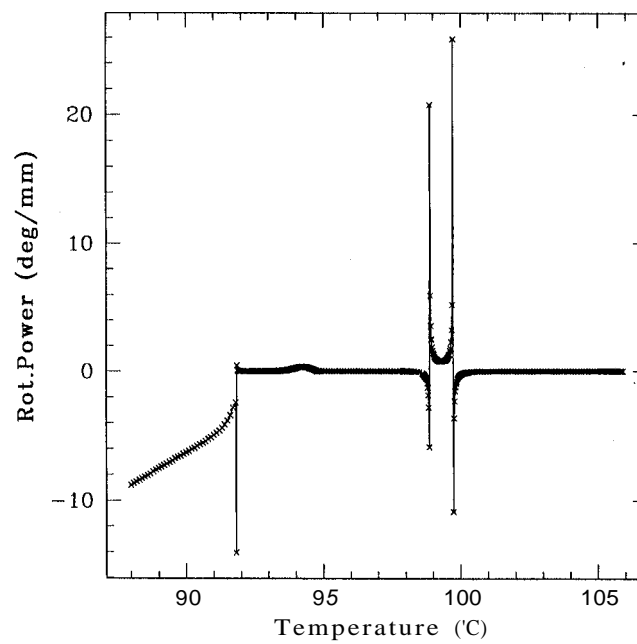


Fig. 4.10: The temperature variation of the theoretically calculated optical rotatory power in the different phases. The wave length of the light used in calculation is 632.8 nm corresponding to a He-Ne laser beam.
